366 *KSME International Journal, Vol. 15, No. 3, pp. 366~373, 2001*

A Numerical Study of Shock Wave/Boundary Layer Interaction in a Supersonic Compressor Cascade

Dong Joo Song*†
Professor, School of Mechanical Engineering, Yeungnam University
Hyun Chul Hwang, Young In Kim
Graduate Student, Graduate School of Mechanical Engineering, Yeungnam University

A numerical analysis of shock wave/boundary layer interaction in transonic/supersonic axial flow compressor cascade has been performed by using a characteristic upwind Navier-Stokes method with various turbulence models. Two equation turbulence models were applied to transonic/supersonic flows over a NACA 0012 airfoil. The results are superion to those from an algebraic turbulence model. High order TVD schemes predicted shock wave/boundary layer interactions reasonably well. However, the prediction of SWBLI depends more on turbulence models than high order schemes. In a supersonic axial flow cascade at M=1.59 and exit/inlet static pressure ratio of 2.21, $k-\omega$ and Shear Stress Transport (SST) models were numerically stables. However, the $k-\omega$ model predicted thicker shock waves in the flow passage. Losses due to shock/shock and shock/boundary layer interactions in transonic/supersonic compressor flowfields can be higher losses than viscous losses due to flow separation and viscous dissipation.

Key Words : $k-\omega$ Model, $k-\varepsilon$ Model, SST Model, Transonic/Supersonic Cascade, TVD Schemes, Shock Wave/Boundary-Layer Interaction (SWBLI)

1. Introduction

Pursuit of advanced aircraft engine performance with high pressure ratio and smaller engine size increased the aerodynamic loading in each compressor stage. The flow velocity inside cascade increased to transonic or supersonic speeds under such conditions, and the high speed caused shock waves and shock wave/boundary layer interactions. Shock wave/turbulent boundary layer interactions frequently occur inside transonic/supersonic cascade flowfields due to the leading edge shock wave impinging onto the developed boundary layer on the suction surface. A shock wave inside the cascade significantly changes aerodynamic performance by increasing total pressure loss, momentum loss, and displacement thickness on the blade surfaces. Various upwind schemes have been proposed by many researchers to solve complex compressible flowfields accurately (e.g. Yee (1989), Gorski et al. (1985), Thomas and Walters (1987) and Shuen (1992)). Yee (1989) modified the flux terms of Harten's (1984) symmetric Total Variation Diminishing (TVD) to reduce dissipation error. Gorski et al. (1985) analyzed a ramp flow by averaged flowfield/$k-\varepsilon$ equations using implicit TVD schemes of Osher and Charkravarthy (1983). Thomas and Walters (1987) studied shock wave/boundary layer interactions using Van Leer's spell out FVS (Van Leer, 1982) and Roe's (1981) approximate Riemann solvers with Flux Difference Splitting (FDS). They solved the reaulting systems of equations by using LU de-

† First Author
* Corresponding Author,
E-mail : djsong@yu.ac.kr
TEL : +82-53-810-2449 ; **FAX** : +82-53-813-3703
Professor, School of Mechanical Engineering, Yeungnam University, Gyongsan 712-160, Korea. (Manuscript **Recevied** June 15, 2000; **Revised** December 18, 2000)

composition. In this analysis, characteristic upwind flux difference splitting method (Lombard et al., 1983, Kwon et al., 1994, and Kim et al., 1996) has been used to include various flux limiters in second order TVD schemes. Two equation turbulence models-Abe et al. 's $k-\varepsilon$ model, Wilcox's $k-\omega$ model, and Menter's Shear Stress Transport (SST) model-have been compared with the Baldwin-Lomax algebraic turbulence model.

2. Numerical Analysis

Two-dimensional/compressible Navier-Stokes equations in general curvilinear coordinates can be written as follows

$$\frac{\partial q}{\partial t}+\frac{\partial F}{\partial x}+\frac{1}{y}\frac{\partial yG}{\partial y}=\frac{\partial F_v}{\partial x}+\frac{\partial G_v}{\partial y}+S \quad (1)$$

where conservative variable q, inviscid fluxes F, G, and viscous fluxes F_v, G_v are given in terms of primitive variables by

$$q=\begin{bmatrix}\rho\\ \rho u\\ \rho v\\ \varepsilon_t\\ \rho k\\ \rho\phi\end{bmatrix}\quad F=\begin{bmatrix}\rho u\\ \rho u^2+p\\ \rho uv\\ u(\varepsilon_t+p)\\ \rho uk\\ \rho u\phi\end{bmatrix}\quad yG=\begin{bmatrix}y\rho v\\ y\rho uv\\ y\rho v^2+\bar{y}p\\ yv(\varepsilon_t+p)\\ y\rho vk\\ y\rho v\phi\end{bmatrix}$$

$$F_v=\begin{bmatrix}0\\ \tau_{xx}\\ \tau_{yx}\\ u\tau_{xx}+v\tau_{yx}-q_x\\ (\mu+\frac{\mu_t}{\rho_k})k_x\\ (\mu+\frac{\mu_t}{\sigma_\phi})\phi_x\end{bmatrix}\quad G_v=\begin{bmatrix}0\\ \tau_{xy}\\ \tau_{yy}\\ u\tau_{xy}+v\tau_{yy}-q_y\\ (\mu+\frac{\mu_t}{\rho_k})k_y\\ (\mu+\frac{\mu_t}{\sigma_\phi})\phi_y\end{bmatrix}$$

S is the source term vector for the turbulence model, and ϕ is the dissipation rate of turbulent kinetic energy (i. e. ε in the $k-\varepsilon$ turbulence model or specific dissipation rate, ω, in the $k-\omega$ model). Volumetric total energy and volumetric internal energy are

$$\varepsilon_t=e+\frac{1}{2}\rho(u^2+v^2),\quad e=\frac{p}{\gamma-1}$$

The effective stress tensor and the effective heat flux vector are given by

$$\tau_{ij}=\tau_{ij}^l-\overline{\rho u_i''u_j''}=(\mu_l+\mu_t)\left[\left(\frac{\partial u_i}{\partial x_j}+\frac{\partial u_j}{\partial x_i}\right)-\frac{2}{3}\delta_{ij}\frac{\partial u_l}{\partial x_l}\right]-\frac{2}{3}\delta_{ij}\rho k$$

$$q_i=-\chi\frac{\partial T}{\partial x_i}+\overline{\rho u_i''e''}=-C_p\left(\frac{\mu_l}{Pr_l}+\frac{\mu_t}{Pr_t}\right)\frac{\partial T}{\partial x_i}$$

The Conservative Supra Characteristic Method (CSCM) upwind flux difference splitting method utilizes the properties of a similarity transformation based on the conservative variable $\tilde{q}$, the primitive variable , and the characteristic variable q.

$$\begin{aligned}\partial_\xi F=\overline{A}\,\partial_\xi q&=\overline{M}\;\overline{T}\;\overline{\Lambda}\;\overline{T^{-1}}\;\overline{M^{-1}}\partial_\xi q\\ &=\overline{M}\;\overline{T}\;\overline{\Lambda}\;\overline{T^{-1}}\partial_\xi\tilde{q}=\overline{M}\;\overline{A'}\partial_\xi\tilde{q}\\ &=\overline{M}\;\overline{T}\;\overline{\Lambda}\partial_\xi\tilde{q}\end{aligned}\quad (2)$$

where $\overline{\Lambda}$ is a diagonal matrix whose diagonal elements correspond to the eigenvalues of the jacobian matrix. Variables q, $\tilde{q}$, and q are related as follows:

$$\partial\tilde{q}=\overline{M^{-1}}\partial q,\ \partial q=\overline{T^{-1}}\partial\tilde{q} \quad (3)$$

$\overline{T}^{-1}$ is a transformation matrix chosen somewhat arbitrarily by considering scaling that leads to logarithmic difference approximations for density, pressure, and Mach number. The characteristic variables can be obtained from the primitive variables through the following relation

$$T^{-1}(\overline{A'}\Delta\tilde{q})=T^{-1}(\overline{T}\;\overline{\Lambda}T^{-1})\Delta\tilde{q}=\overline{\Lambda}\Delta\tilde{q} \quad (4)$$

The inviscid flux can be divided into ΔF^+ and ΔF^- using a diagonal truth function matrix $D^\pm$ and Eq. (2) can be written as

$$\begin{aligned}\Delta F&=\overline{M}\;\overline{A'}\Delta\tilde{q}=\overline{M}(\overline{T}\,I\,\overline{T^{-1}})\,\overline{A'}\Delta\tilde{q}\\ &=\overline{M}\;\overline{T}(D^+-D^-)\,\overline{T^{-1}}\;\overline{A'}\Delta\tilde{q}=\Delta F^+-\Delta F^-\end{aligned}\quad (5)$$

where $D^+=\frac{1}{2}\left[1+\frac{\Lambda}{|\Lambda|}\right]$, $D^-=\frac{1}{2}\left[1-\frac{\Lambda}{|\Lambda|}\right]$

Using the relation $\overline{A'}\Delta\tilde{q}=\tilde{M}^{-1}\Delta q$, Eq. (5) can be rewritten as

$$\Delta F^\pm=\overline{M}\;\overline{T}D^\pm\overline{T^{-1}}\tilde{M}^{-1}\Delta q=\tilde{A}^\pm\Delta q \quad (6)$$

Equation (6) satisfies the property 'U' of Roe and thus the flux vectors are conserved. The formulation becomes complex due to the transformation matrices $\overline{M}$, $\overline{T}$ and $\tilde{M}^{-1}$. However, the differencing scheme has the representation of the convective flow propagation through these

matrices and naturally allows easy characteristic boundary conditions via modified $\overline{T'^{-1}}$ (Lombard et al (1983)). The implicit finite difference equation can be discretized using one sided differencing, depending on the sign of eigenvalues of the Jacobian matrices. Using approximate factorization with diagonal dominance, the equations are successively solved along ξ- and η-directions.

3. High Resolution Scheme

3.1 Flux extrapolation method

For second order accuracy of the inviscid terms in the explicit part, we used the Fromm scheme ($\eta=0$) with minmod limiters (Hirsch, 1990).

$$\Delta F_i^* = F_{i+\frac{1}{2}}^* - F_{i-\frac{1}{2}}^* \tag{7}$$

$$\begin{aligned}\Delta F_{i+\frac{1}{2}}^* = F_{i+\frac{1}{2}}^* &- \frac{(1-\eta)}{4}(\tilde{\Delta}_{j+\frac{3}{2}}F^-) \\ &- \frac{(1+\eta)}{4}(\tilde{\Delta}_{j+\frac{1}{2}}F^-) \\ &- \frac{(1+\eta)}{4}(\tilde{\Delta}_{j+\frac{1}{2}}F^+) \\ &- \frac{(1-\eta)}{4}(\tilde{\Delta}_{j-\frac{1}{2}}F^+)\end{aligned} \tag{8}$$

$\tilde{\Delta}$, Δ : Minmod limiter

$\min \mathrm{mod}(x, \omega y) = s \max[0, \min(|x|, \omega sy)]$, $s = \mathrm{sign}(x)$

and we also used the Chakravarthy-Osher scheme ($\eta=1$) when necessary.

3.2 Flux modified method

The TVD method of Yee-Harten (1987) can be written as

$$\tilde{F}_{i+\frac{1}{2}} = \frac{1}{2}[F_i + F_{i+1} + R_{i+\frac{1}{2}}\phi_{i+\frac{1}{2}}] \tag{9}$$

where R represents the eigenvectors of Jacobian matrix and vector ϕ is given by

$$\phi : \phi_{i+\frac{1}{2}}^l (l=1, 2, 3, \cdots, m)$$

The Function ϕ, modified by Yee for diffusion, is given by

$$\begin{aligned}\phi_{i+\frac{1}{2}}^l = &\frac{1}{2}\varphi(a_{i+\frac{1}{2}}^l)(g_i^l + g_{i+1}^l) - \varphi(a_{i+\frac{1}{2}}^l \\ &+ \gamma_{i+\frac{1}{2}}^l)\alpha_{i+\frac{1}{2}}^l\end{aligned} \tag{10}$$

$$\alpha_{i+\frac{1}{2}}^l = R_{i+\frac{1}{2}}^{-1} \frac{Q_{i+1} - Q_i}{\frac{1}{2}(J_{i+1} + J_i)},$$

$$g_i^l = S \cdot \max[0, \min(|\alpha_{i+\frac{1}{2}}^l|, S \cdot \alpha_{i-\frac{1}{2}}^l)]$$

a : eigenvalue of Jacobian matrix, α : characteristic variable

Q : conservative variable, J : jacobian transformation

$$S = \mathrm{sing}(\alpha_{i+\frac{1}{2}}),\ \varphi(z) = \begin{cases} \dfrac{(z^2+\varepsilon^2)}{2\varepsilon} & : |z| < \varepsilon \\ |z| & : |z| \geq \varepsilon \end{cases}$$

$$\gamma_{i+\frac{1}{2}}^l = \frac{1}{2}\varphi(a_{i+\frac{1}{2}}^l) = \begin{cases} (g_{i+1}^l - g_i^l)/\alpha_{i+\frac{1}{2}}^l & : a_{i+\frac{1}{2}} \neq 0 \\ 0 & : a_{i+\frac{1}{2}} = 0 \end{cases}$$

4. Turbulence Models

In this paper we employed Abe et al. 's. (1992), $k-\varepsilon$ turbulence model, Wilcox's (1988, 1993) $k-\omega$ turbulence model and menter's (1994) SST model.

4.1 Abe et al. 's $k-\varepsilon$ model

The $k-\varepsilon$ turbulence model proposed by Abe et al. employed the Kolmogorov velocity scale $u_\varepsilon = (\nu\varepsilon)^{1/4}$ instead of the conventional friction velocity u_τ. The source terms, model coefficients, and damping functions can be written as

$$S = \begin{bmatrix} P_k - \rho\varepsilon \\ c_1 f_1 \frac{\varepsilon}{k} P_k - c_2 f_2 \frac{\rho\varepsilon^2}{k} \end{bmatrix},\ \mu_t = c_\mu f_\mu \rho \frac{k^2}{\varepsilon}$$

$\sigma_k = 1.6$, $\sigma_\phi = 1.6$, $c_1 = 1.9$, $c_2 = 1.9$,

$f_\mu = [1 - \exp(-y^*/14)]^2 \times [1 + (5/R_t^{3/4}) \exp[(R_t/200)^2]]$ (11)

$f_1 = 1$, $f_2 = [1 - \exp(-y^*/3.1)]^2 \times [1 - 0.3 \exp[-(R_t/6.5)^2]]$

$y^* = \rho u_\varepsilon y/\mu$, $u_\varepsilon = (\mu\varepsilon/\rho)^{1/4}$

$$P_k = \mu_t\left[\frac{1}{2}\left(\frac{\partial u_i}{\partial x_j} + \frac{\partial u_j}{\partial x_i}\right)^2 - \frac{2}{3}\left(\frac{\partial u_1}{\partial x_1}\right)^2\right] - \frac{2}{3}\rho k \frac{\partial u_1}{\partial x_1},\ R_t = \frac{\rho k^2}{\mu\phi}$$

This incompressible $k-\varepsilon$ model has been extended to a compressible flow problem by Kim and Song (2000).

4.2 Wilcox's $k-\omega$ model

Wilcox's $k-\omega$ model in the viscous sublayer zone predicts the skin friction coefficient more accurately for strong adverse pressure gradient

flows and is numerically more stable than the k $-\varepsilon$ model. The initial value of ω has significant effects on boundary layers in the k$-\omega$ model (Wilcox, 1988). However, it is not easy to generate ω. The k$-\varepsilon$ model is not sensitive to the freestream value of ε. The Source terms, model coefficients, and damping functions can be written as

$$S=\begin{bmatrix} P_k-\beta^* \rho\omega k \\ \alpha\frac{\omega}{k}P_k-\beta\rho^2\omega \end{bmatrix} \quad (12)$$

$$\mu_t=\sigma\gamma^*\frac{k}{\omega},\ \sigma_\omega=2.0,\ \sigma_k=2.0,\ \alpha=\frac{5}{9},$$

$$\beta=\frac{3}{40},\ \beta^*=\frac{9}{100},\ \gamma^*=1$$

4.3 Menter's SST model

Baseline model which is a k$-\omega$ model near a wall becomes a k$-\varepsilon$ model at farfield by using the blending function F_1. The transport equations for turbulent kinetic energy, specific dissipation rate of turbulence, and the blending function can be written as follows

$$\frac{\partial\rho k}{\partial t}+\frac{\partial}{\partial x_j}[\rho u_j k-(\mu+\sigma_k\mu_t)\frac{\partial k}{\partial x_j}] = P_k-\beta^*\rho\omega k \quad (13)$$

$$\frac{\partial\rho\omega}{\partial t}+\frac{\partial}{\partial x_j}[\rho u_j\omega-(\mu+\sigma_\omega\mu_t)\frac{\partial\omega}{\partial x_j}] = P_\omega-\beta\omega^2+2(1-F_1)\frac{\rho\sigma_{\omega2}}{\omega}\frac{\partial k}{\partial x_j}\frac{\partial\omega}{\partial x_j} \quad (14)$$

$$F_1=\tanh\{(\min[\max[\frac{2\sqrt{k}}{0.009\omega y};\frac{500\mu}{\rho y^2\omega}],\frac{4\rho\sigma_{\omega2}k}{CD_{k\omega}y^2}])^4\}$$

$$CD_{k\omega}=(\max[\frac{2\rho\sigma_{\omega2}}{\omega}\frac{\partial k}{\partial x_j}\frac{\partial\omega}{\partial x_j};10^{-20}]$$

$\sigma_{\omega2}$: model constant

In the SST model, production terms of specific dissipation and eddy viscosity can be written as

$$P_\omega\equiv2\gamma\rho(S_{ij}-\omega S_{nn}\delta_{ij}/3)S_{ij}\approx\gamma\rho\Omega^2$$

$$\mu_t=\frac{\rho k/\omega}{\max[1;\Omega F_2/(\alpha_1\omega)]}$$

$$\alpha_1=0.31,\ \beta^*=0.09,\ k=0.41,$$

$$F_2=\tanh\{(\max[\frac{2\sqrt{k}}{0.009\omega y};\frac{500\mu}{\rho y^2\omega}])^2\} \quad (15)$$

S_{ij} : mean strain rate, γ : model coefficient

where F_2 and Ω are the auxiliary function and the absolute value of vorticity, respectively.

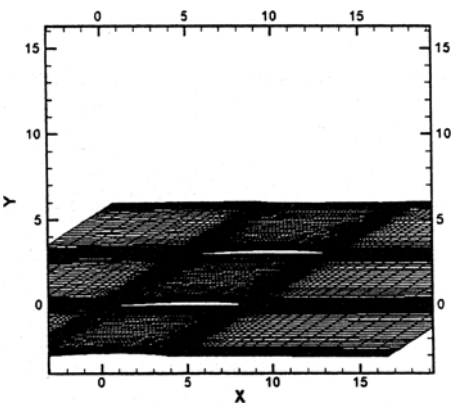

Fig. 1 Grid system (130×90, H-type)

5. Boundary Conditions and Grid System

An H-type grid was constructed by using elliptic P. D. E. grid generation techniques. A stretching function was used to cluster grids near the wall. The grid system was 130×90 in the longitudinal and the normal directions of the flowfield, respectively. Incoming flow properties were prescribed using freestream values. At the outflow boundary, back-pressure was prescribed. No-slip and adiabatic wall conditions were used on the wall (Fig. 1).

6. Results and Discussion

6.1 Verification of high resolution schemes and turbulence models

The first case considered here to show the accuracy of the schemes is a transonic flow over NACA0012 airfoil with $M_\infty=0.8$ and $\alpha=1.25°$, where M_∞ is the freestream Mach number and α is the angle of attack. Figure 2 shows the plots of pressure coefficient distributions using a first-order and high-order schemes.

Yee-Harten's and Fromm's schemes show that shock waves can be predicted to within 3 grid points on the upper surface of the airfoil, and these results are compare well with those of Pulliam and Child (1983). Figure 2(a) shows that a non-TVD second-order accuracy scheme

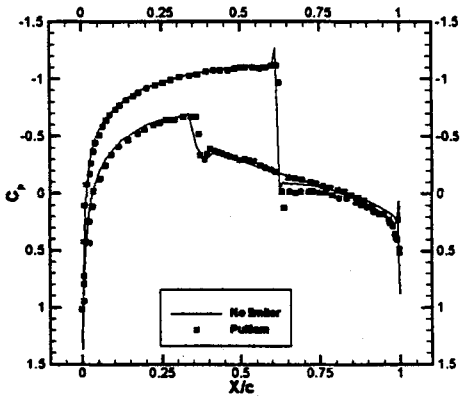

(a) Non-TVD scheme

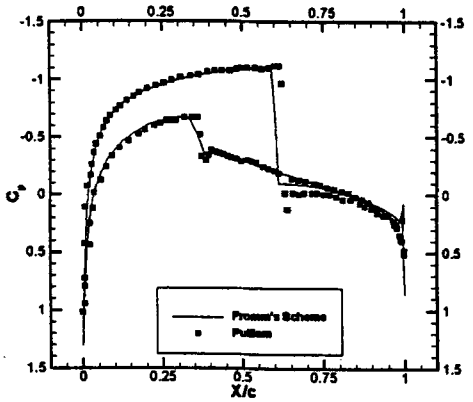

(b) Fromm scheme($\eta=0$, $\omega=3$)

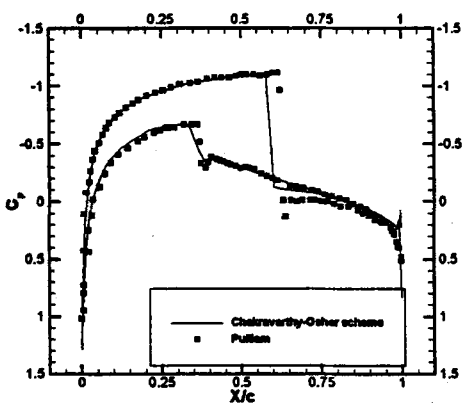

(c) Chakravarthy-Osher scheme($\eta=1$, $\omega=2$)

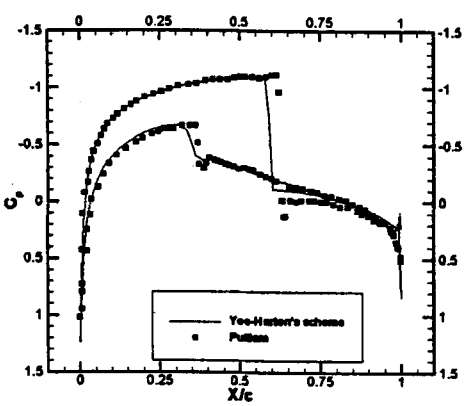

(d) Yee-Harten scheme

Fig. 2 Comparison of computed surface pressure distribution over NACA 0012 airfoil among : (a) No limiter (second Order), (b) Fromm scheme, (c) Chakravarthy-Osher scheme, and (d) Yee-Harten scheme and Pulliam's results ($M_\infty=0.8$, $\alpha=1.25°$)

produces wiggles in the region where oblique shock waves occur. On the contrary, TVD schemes yield a sharp pressure rise without any oscillations near the shock waves (Figs. 2(b)-2 (d)). Yee-Harten's and Fromm's schemes predict the pressure increase within a narrower region than others schemes.

Figure 3 shows the prediction from the selected algebraic and two-equation turbulence models with Fromm's second order flux extrapolation scheme for a NACA0012 airfoil. The two-equation models generally performed well in predicting the shock location and the pressure rise after the shock.

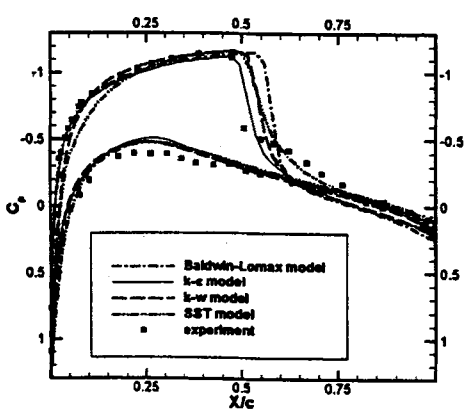

Fig. 3 The validation of turbulence models over NACA 0012 airfoil ($M_\infty=0.8$, $\alpha=2.26°$)

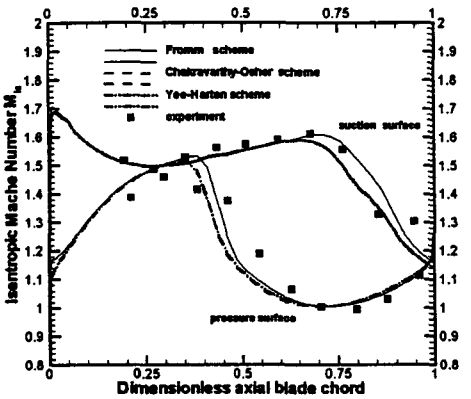

Fig. 4 Comparison of blade isentropic Mach number among high order schemes with k-ε model

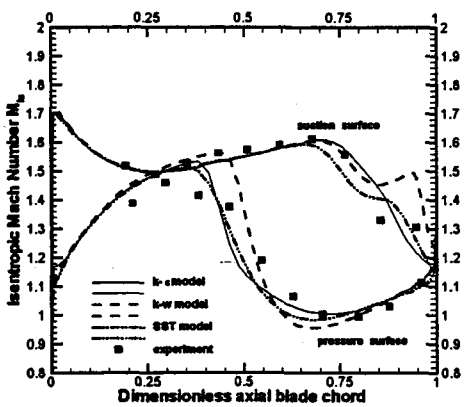

Fig. 5 Comparison of blade isentropic Mach number among various turbulence models

6.2 ARL-SL19 linear cascade flow analysis

Supersonic ARL-SL19 cascade flows at M=1.59 and $p_2/p_1=2.21$ were analyzed by comparing turbulence models with high-resolution schemes. Figure 4 shows the predicted isentropic Mach No. distributions from the second-order accuracy TVD schemes with Abe et al.'s turbulence model. The Fromm scheme accurately predicted the shock location on the suction surface. However, other high-resolution schemes predicted shock locations were upstream of the experimental data.

The isentropic Mach No. distributions from two-equation models agreed with the experimental data as shown in Fig. 5. The SST turbulence model yielded a shock location upstream of the experimental data. Other schemes matched the

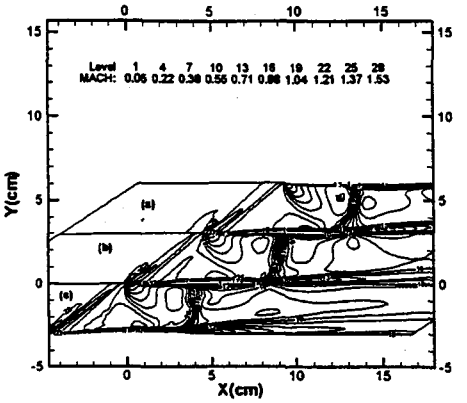

Fig. 6 Mach number contours with Fromm scheme: (a) k-ε model, (b) k-ε model, and (c) SST model

experimental data. Current turbulence models could not successfully predict the sudden pressure rise due to the reflected shock wave which penetrated the pressure surface boundary layer and formed a shock wave/boundary-layer interaction (SWBLI) zone over the pressure surface. The shock wave predicted by the k$-\omega$ model occurred downstream of the experimental data because this model predicted a thinner boundary layer than other schemes.

Figure 6 shows the predicted isentropic Mach number contours from different turbulence models with the Fromm scheme. The k$-\varepsilon$ turbulence model predicted the shock-wave/turbulent boundary-layer interaction well. The shock types were a λ-shock on the suction surface and a Mach reflection (Y) shock on the pressure surface (Fig. 6(a)). But the k$-\omega$ turbulence model predicted a nearly normal shock structure on the pressure surface and a thicker shock wave in the flow passage (Fig. 6(b)). The k$-\omega$ turbulence model did not predict a gradual pressure increase over the Y-shock region. The SST model predicted a similar flow pattern similm to that of the k$-\varepsilon$ model (Fig. 6(c)).

Figure 7 shows the predicted pressure contours from three different turbulence models with the Fromm scheme. A λ-shock wave was formed near the trailing edge of the suction surface due to a shock-wave from the leading edge impinging onto the turbulent pressure surface boundary

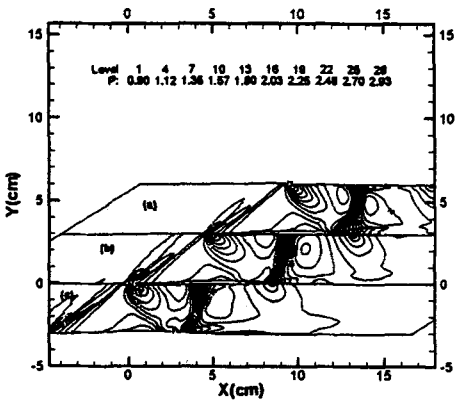

Fig. 7 Pressure contour plot with Fromm scheme : (a) k-ε model, (b) k-ε model, and (c) SST model

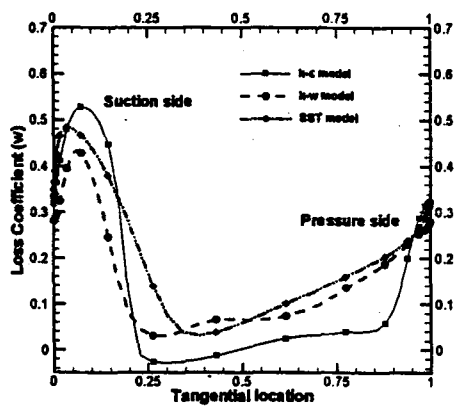

Fig. 8 Total pressure loss coefficient comparison among k-ε model, k-ω model, and SST model

layer.

Figure 8 shows the total pressure loss coefficient near the trailing edge. The peak total pressure losses were observed near the shock-wave/turbulent boundary-layer interaction zone due to viscous and shock losses. The k$-\omega$ turbulence model, which inaccurately predicted the shock-wave/turbulent boundary-layer interaction zone, predicted lower losses than other turbulence models.

7. Conclusions

A characteristic upwind flux difference splitting Navier-Stokes method with high resolution TVD schemes and various turbulence models was developed to analyze transonic/supersonic flowfields. Three two-equation models and a Baldwin-Lomax algebraic model successfully predicted the transonic boundary layer flow around a NACA0012 airfoil at M=0.8. The high-resolution methods accunately captured the shock position. Two-equation turbulence models preduction were better than those of the Baldwin-Lomax algebraic model. A supersonic compressor cascade flowfield at Mach Number 1.59 and an exit/inlet static pressure ratio 2.21 was also analyzed. The prediction of SWBLI in the cascade did not strongly depend on high-resolution methods, but on turbulence models. The Abe et al. 's k$-\varepsilon$ model and the SST model performed better than the k$-\omega$ turbulence model in predicting the pressure variation in interaction regions. However, in the flow passage, the shock thickness from the SST model is a little bit thicker than that of the k$-\omega$ model. The k$-\omega$ model and the SST model were numerically stable. The k$-\omega$ model predicted thinner boundary layers than the other two-equation turbulence models and did not predict the shock position accurately. From current numerical experiments, we confirmed that most of the total pressure losses in supersonic compressor cascades were related to SWBLI. Accordingly, more efficient and accurate turbulence modeling is needed for compressor cascade design or performance analysis.

References

Abe, K., Nagano, N. and Kondoh, T., 1992, "An Improved Model for Prediction of Turbulent Flows with Separation and Reattachment," *Trans. JSME. Ser.* B, 58, pp. 3003~3010.

Chakravarthy, S. R. and Osher, S., 1983, "Upwind Schemes and Boundary Layer Conditions with Applications to Euler Equations in General Geometries," *J. Comp. Phys.*, Vol. 50, pp. 447~481.

Gorski, J. J., Chakravarthy, S. R., and Goldberg, U. C., 1985, "High Accuracy TVD Schemes for the Equations of Turbulence," *AIAA*, Paper No. 85-1665.

Harten, A., 1984, "On a Class of High Resolution Total-Variation-Stable Finite-Difference Schemes," *SIAM J. Num. Anal.*, Vol. 21, pp. 1~23.

Hirsch, C., 1990, *Numerical Computation of Internal and External Flows,* Vol. 2, John Wiley & Sons Ltd.

Song, D. J. and Kim, S. D., 2000, "A Comparative Numerical Study of Shock/Boundary-Layer Intereraction using Navier-Stokes," *Computational Fluid Dynamics Journal*, Vol. 9, to be printed

Kim, S. D., Kwon, C. O., Song, D. J., and Sa, J. Y., 1994, "Performance Enhancement Study Using Passive Control of Shock-Boundary Layer Interaction in a Transonic/Supersonic Compressor Cascade," *KSME Journal*, Vol. 20, No. 9, pp. 2944~2952.

Kwon, C. O., Song, D. J., and Kang, S. H., 1994, "Compressor Cascade Flow Ananysis by Using Upwind Flux Difference Splitting Method," *KSME Journal*, Vol. 18, No. 3, pp. 635~661.

Lombard, C. K., Bardina, J., Venkatapathy, E., and Oliger, J., 1983, "Multi-Dimensional Formulation of CSCM-An Upwind Flux Difference Eigenvector Split Method for the Compressible Navier-Stokes Equations," AIAA-83-1859cp.

Menter, F. R., 1994, "Two-Equation Eddy Viscosity Turbulence Models for Engineering Applications," *AIAA J.*, Vol. 32, pp. 1299~1310.

Pulliam, T. H. and Childs, R. E., 1983, "An Enhanced Version of an Implicit Code for the Euler Equation," AIAA-83-0344.

Roe, P. L., 1981, "Approximate Riemann solvers, Parameter Vectors and Difference Scheme," *J. Comp. Phys.*, Vol. 43, pp. 357~372.

Shuen, J. S., 1992, "Upwind Differencing and LU Factorization for Chemical Non-equilibrium Navier-Stokes Equations," *J. Comp. Phys*, Vol. 99, pp. 233~250.

Thomas, J. L. and Walters, R. W., 1987, "Upwind Relaxation Algorithms for the Navier-Stokes Equation," *AIAA J.*, Vol. 25, pp. 527~534.

Van Leer, B., 1982, "Flux Vector Splitting for Euler Equations," *Lecture Notes in Physics*, Vol. 170, pp. 501~512.

Wilcox, D. C., 1988, "Reassessment of the Scale-Determining Equation for Advance Turbulence Models," *AIAA J.*, Vol. 26, No. 11, pp. 1299~1310.

Wilcox, D. C., 1993, "Turbulence Modeling for CFD," DCW Industries, Inc., 5354 Palm Drive, La Canada, Calif.

Yee, H. C. and Harten, A., 1987, "Implicit TVD Schemes for Hyperbolic Conservation Laws in Curvilinear Coordinates," *AIAA J.*, Vol. 25, No. 2, pp. 266~274.

Yee, H. C., 1989, "A Class of High-Resolution Explicit and Implicit Shock-Capturing Methods," NASA Technical Memorandum 101088.